Published for SISSA by Springer

Received: *June 4, 2025*
Accepted: *September 26, 2025*
Published: *November 4, 2025*

New measurement of D^0 and D^+ meson masses with the KEDR detector

The KEDR collaboration

V.V. Anashin et al.

Full author list at the end of the paper

E-mail: I.V.Ovtin@inp.nsk.su

Abstract: Using the $4.9\,\mathrm{pb}^{-1}$ statistics collected at the peak of the $\psi(3770)$ resonance with the KEDR detector at the VEPP-4M electron-positron collider, we measured the masses of the neutral and charged D mesons:

$$M_{D^0} = 1865.100 \pm 0.210_{\mathrm{stat}} \pm 0.046_{\mathrm{syst}}\,\mathrm{MeV},$$
$$M_{D^+} = 1869.560 \pm 0.288_{\mathrm{stat}} \pm 0.109_{\mathrm{syst}}\,\mathrm{MeV}.$$

Keywords: Charm Physics, e^+-e^- Experiments

ArXiv ePrint: 2506.02421

https://doi.org/10.1007/JHEP11(2025)001

JHEP11(2025)001

Contents

1 Introduction

Neutral and charged D mesons are the ground states in the family of open charm mesons. Measurement of their masses provides a mass scale for the heavier excited states. In addition, a precise measurement of the D^0 meson mass can help to understand the nature of the narrow $X(3872)$ state, which, according to some models, is a bound state of D^0 and D^{*0} mesons and has a mass very close to the sum of the D^0 and D^{*0} meson masses [1].

Currently, as quoted by the Review of Particle Physics (PDG) [2], the world average D^0 mass is $M_{D^0} = 1864.84 \pm 0.05$ MeV. The most precise measurement was made using CLEO data (2014), which reported $M_{D^0} = 1864.845 \pm 0.025_{\rm stat} \pm 0.057_{\rm syst}$ MeV [3]. The another less precise measurements were made by the BABAR(2013) [4], LHCb(2013) [5], CLEO(2007) [6] and KEDR(2010) [7] collaborations. The world average D^+ mass is $M_{D^+} = 1869.50 \pm 0.40$ MeV and the most precise determination of the D^+ mass made by the KEDR collaboration $M_{D^+} = 1869.53 \pm 0.49_{\rm stat} \pm 0.20_{\rm syst}$ MeV [7].

The goal of our present measurement is to determine the masses of neutral and charged D mesons with a precision better than that of our result published in [7]. After a long shutdown from April 2011 to May 2014 a further $4\,{\rm pb}^{-1}$ of data has been collected. During this shutdown a second layer of aerogel Cherenkov counters was installed.

2 VEPP-4M collider and KEDR detector

The experiment was performed with the KEDR detector [8, 9] at the electron-positron collider VEPP-4M [10]. It operates in the wide range of beam energy from 1 to 6 GeV. The circumference of the VEPP-4M ring is 366 m. The peak luminosity of the collider at

JHEP11(2025)001

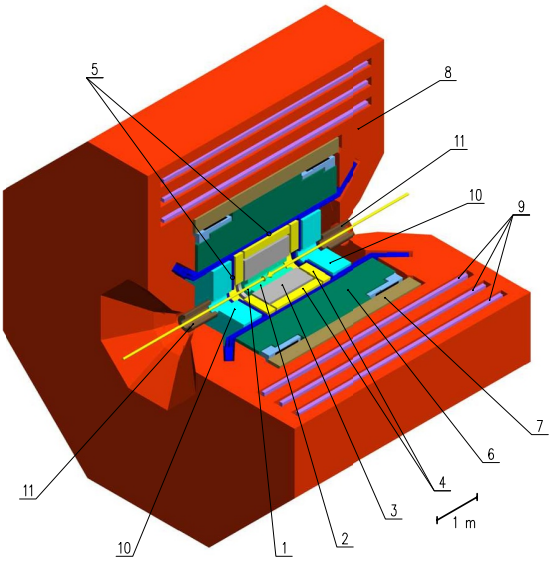

Figure 1. The central part of the KEDR detector: (1) vacuum chamber of the collider; (2) vertex detector; (3) drift chamber; (4) aerogel threshold Cherenkov counters; (5) time of flight counters; (6) liquid krypton barrel calorimeter; (7) superconductive solenoid; (8) magnet yoke; (9) muon chambers; (10) endcap CsI calorimeter; (11) compensating coil.

energy 1.85 GeV in operation mode with 2×2 bunch at a beam current of 3.0 mA reaches $2 \times 10^{30}\,\mathrm{cm}^{-2}\,\mathrm{s}^{-1}$. One of the main features of the VEPP-4M is its capability to precisely measure the beam energy using the resonant depolarization method [11]. The resonant depolarization method is based on the measurement of the spin precession frequency of the polarized beam and has a precision 10^{-6}.

A schematic diagram of the KEDR detector is shown in figure 1. The KEDR detector includes a tracking system consisting of a vertex detector and a drift chamber, a particle identification (PID) system of aerogel threshold Cherenkov counters and time of flight scintillation counters, and electromagnetic calorimeter based on liquid krypton in barrel part and CsI crystals in endcap, and muon system based on streamer tubes. The longitudinal magnetic field of 0.6 T in the detector is provided by a superconducting solenoid. The iron core of the magnet is used by the muon system as an absorber. For investigation of two-photon processes, the detector includes the modules of a system for detecting the scattered electrons and positrons. The online luminosity measurement is provided by two independent single bremsstrahlung monitors.

Charged tracks are reconstructed in the drift chamber (DC) and vertex detector (VD). The DC [12] has a cylindrical shape of 1100 mm length, an outer radius of 535 mm and is filled with pure dimethyl ether. The VD [13] is installed between the vacuum chamber and DC and increases the solid angle accessible to the tracking system to 98%. The VD consists of 312 cylindrical drift tubes aligned in 6 layers. It is filled with an Ar + 30%CO_2 gas mixture. The entire volume of the DC is divided into 7 cylindrical superlayers: 4 axial layers and 3 stereo-layers to measure track coordinates along the beam axis. Each superlayer consists of cells with 6 signal anode wires. A particle that crosses all the DC

JHEP11(2025)001

superlayers gives 42 coordinate measurements. There are also additional 6 coordinate measurements in the VD. The degradation of the momentum resolution of the tracking system is observed during the experiment on the KEDR detector. For data collected in 2004 it is $\sigma_p^2/p^2 = 2.9\%^2 + (4.5\% \times p[GeV])^2$, while for data collected in 2016 it is $\sigma_p^2/p^2 = 3.5\%^2 + (5.5\% \times p[GeV])^2$. This degradation influence the efficiency of D-mesons reconstruction.

Scintillation counters of the time-of-flight system (TOF) are used in a fast charged trigger and for identification of the charged particles by their flight time. The TOF system consists of 32 plastic scintillation counters in the barrel part and in each of the endcaps. The flight time resolution is about 350 ps, which corresponds to π/K separation at the level of more than two standard deviations for momenta up to 650 MeV/c.

Aerogel Cherenkov counters (ACC) [14] are used for particle identification in the momentum region not covered by the TOF system and ionizations measurements in DC. ACC uses aerogel with the refractive index of 1.05 and wavelength shifters for light collection. The system design includes 160 counters in the endcap and barrel parts, each arranged in two layers. The system permits π/K separation in momentum range from 0.6 to 1.5 GeV/c.

The muon system [15] is used to reject cosmic muons. It consists of three layers of streamer tubes with 74% solid angle coverage, the total number of channels is 544.

During the long shutdown from April 2011 to May 2014, repairs were carried out on the detector equipment. A second layer of the aerogel Cherenkov counters was installed. This allowed the use identification system for the π/K separation in the D meson masses analysis for data collected after 2014.

3 Data samples

The analysis is based on two experimental data samples collected at the peak of the $\psi(3770)$ resonance with total integral luminosity of 4.9 pb^{-1}. The first data sample of 0.9 pb^{-1} was collected in 2004. That data were used to obtain the result published in [7], which is presented in the PDG tables [2]. For this result, the systematic uncertainty due to initial state radiation corrections (ISR) dominates the total systematic uncertainty. It is determined by the accuracy of the energy dependence of the cross section $\sigma(e^+e^- \to D\bar{D})$. Since then BES-III has published new results [16, 17] and consequently as well as studying the new data the data from [7] is reanalysed. The second data sample of 4.0 pb^{-1} was collected in 2016–2017 after the long shutdown of the KEDR detector.

4 Measurement method

The measurement of D meson masses is performed using $e^+e^- \to D\bar{D}$ production near the threshold with full reconstruction of one of the D mesons. Neutral D mesons are reconstructed in the $K^-\pi^+$ (and charge conjugates) final state ($\mathcal{B}(D^0 \to K^-\pi^+) = (3.95 \pm 0.03)\%$), charged D mesons are reconstructed in the $K^-\pi^+\pi^+$ (and charge conjugates) final state ($\mathcal{B}(D^+ \to K^-\pi^+\pi^+) = (9.38 \pm 0.16)\%$). To increase the data sample, the collider is operated at the peak of the $\psi(3770)$ resonance. The production cross sections at $\psi(3770)$ energy are $\sigma(D^0\bar{D}^0) = 3.61 \pm 0.01 \pm 0.04$ nb and $\sigma(D^+D^-) = 2.83 \pm 0.01 \pm 0.03$ nb [16, 17].

JHEP11(2025)001

The invariant mass of the D meson can be calculated as

$$M_{bc} = \sqrt{E^2_{\rm beam} - \left(\sum_i \vec{p_i}\right)^2}, \tag{4.1}$$

(so-called beam-constrained mass), where $E_{\rm beam}$ is the beam energy, $\vec{p_i}$ are the momenta of the D decay products. The use of the beam-constrained approach for the mass determination causes the mass shift due to the difference of the beam energy and the mean energy of the meson produced. This difference appears because of ISR and, additionally, because of the energy spread when the data are collected aside of the cross section maximum. Besides, final state radiation (FSR) causes the difference between the meson momentum and the momentum of its decay products. All these effects are accounted in simulation of the $M_{\rm bc}$ line shape.

The uncertainty associated with imprecise knowledge of the beam energy is not significant in the case of VEPP-4M. The beam constrained mass calculated this way is determined more precisely than in the case when the D energy is obtained from the energies of the decay products. The precision of the $M_{\rm bc}$ measurement in one event is

$$\sigma^2(M_{bc}) = \frac{\sigma^2_W}{4} + \left(\frac{p_D}{M_D}\right)^2 \sigma^2_{p_D} = \frac{\sigma^2_W}{4} + 0.02\sigma^2_{p_D}, \tag{4.2}$$

where σ_W is the center-of-mass (CM) energy spread. The contribution of the momentum resolution is suppressed significantly due to small D momentum ($p_D \simeq$260 MeV).

In addition to M_{bc}, D mesons are effectively selected by the CM energy difference

$$\Delta E = \sum_i \sqrt{(m_i^2 + p_i^2)} - E_{\rm beam}, \tag{4.3}$$

where m_i and p_i are the masses and momenta of the D decay products. For a signal event ΔE is close to zero. In our analysis, we select a relatively wide region of M_{bc} and ΔE: $M_{bc} > 1700\,$MeV, $|\Delta E| < 300\,$MeV. Then a fit of the event density is performed with the D mass as one of the parameters, with the background contribution taken into account. The background in our analysis comes from the random combinations of tracks of the continuum process $e^+e^- \to q\bar{q}(q = u, d, s)$ and from other decays of D mesons.

While calculating $M_{\rm bc}$, we employ a kinematic fit with the $\Delta E = 0$ constraint. It is done by minimizing the χ^2 function formed by the momenta of the daughter particles

$$\chi^2 = \sum_i \frac{(p'_i - p_i)^2}{\sigma^2_{p_i}} \tag{4.4}$$

where p_i and σ_{p_i} are the measured momenta of the daughter particles and their errors obtained from the track fit, respectively, which are corrected by contributions described in more detail below, and p'_i are the fitted momenta which satisfy the $\Delta E(p'_i) = 0$ constraint.

For the D^0 meson mass measurement in addition to variables $M_{\rm bc}$ and ΔE we include the variable $\Delta|p|$ which also allows one to efficiently separate the signal from the background, thus improving the overall statistical accuracy of the measurement. $\Delta|p|$ is the difference of the absolute values of momenta for D^0 decay products in the CM frame. We use the fact that $M_{\rm bc}$ resolution depends strongly on decay kinematics — it can be up to three times better for

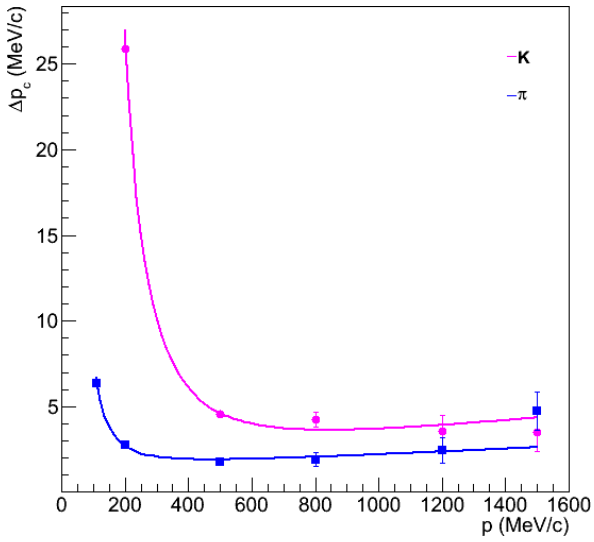

Figure 2. The deviation of reconstructed momentum from the true one in simulation of pions (blue rectangles) and kaons (magenta circles).

events where the daughter particles from D^0 decay move transversely to the direction of the D^0 ($\Delta|p|$ is around zero for these events), than for events where they move along this direction.

The precision of the momentum measurement has direct influence on the D mass measurement. The following corrections are applied to values of reconstructed momenta:

1. First the correction of track momenta due to ionization loss for data is applied based on simulation. We simulated monochromatic particles (pions and kaons) from the center of the detector that traverse the vacuum chamber. The deviation of reconstructed momentum from the true Δp_c one in simulation of pions and kaons is shown in figure 2. To compensate for this effect, a momentum correction was taken into account:

$$\begin{aligned} p_c &= p + \Delta p_c, \\ \Delta p_c &= D/\beta^3 + \kappa p, \end{aligned} \tag{4.5}$$

   where $\beta = p/\sqrt{m^2 + p^2}$, and D, m, κ are free parameters obtained by the fit.

2. Then momentum scale coefficient α is applied (absolute momentum calibration), where α is determined to give average ΔE of the selected D sample for this analysis to be close to zero (i.e. $\langle \Delta E \rangle \sim 0$). The scale coefficient α relates the true track momentum p_{true} and the measured momentum p_c:

$$p_{\text{true}} = \alpha p_c. \tag{4.6}$$

   Then

$$\begin{aligned} M_{bc} &= \sqrt{E_{\text{beam}}^2 - \alpha^2 \left(\sum_i \vec{p_{ci}} \right)^2}, \\ \Delta E &= \sum_i \sqrt{(m_i^2 + \alpha^2 p_{ci}^2)} - E_{\text{beam}}. \end{aligned} \tag{4.7}$$

The most probable α value was determined by several repeated processings of the data sample. As a result the dependence of $|\langle\Delta E\rangle|$ from α is obtained, the minimum of which is closest to zero. The value of α at the minimum is used for further data processing. Since the distribution of ΔE includes the ISR effect $\langle\Delta E\rangle$ is not necessarily zero. For the first and second data samples, as well as for samples D^0 and D^+ in the fit, different values of α are used, which are determined independently.

For each reconstructed D candidate, the corrections (1) and (2) are applied to track momenta and kinematic fit is done to give $\Delta E = 0$. $M_{\rm bc}$ and $\Delta|p|$ are calculated using resulting momenta of kinematic fit. For ΔE, the value, before kinematic fit but with the corrections (1) and (2) are applied, is used.

The description of the momentum resolution in the simulation is adjusted using cosmic tracks. We select cosmic tracks that traverse the vacuum chamber and fit their upper and lower parts separately.

In order to measure the D mass most efficiently, the unbinned maximum likelihood fit procedure is used. The likelihood function has the form:

$$-2\ln\mathcal{L}(\epsilon) = -2\sum_{i=1}^{N}\ln\mathcal{P}(\mathbf{v}_i|\epsilon) + 2N\log\int\mathcal{P}(\mathbf{v}|\epsilon)d\mathbf{v}, \tag{4.8}$$

where N is number of events, $\mathbf{v} = (M_{\rm bc}, \Delta E, \Delta|p|)$ includes the variables that characterize one event, $\mathcal{P}(\mathbf{v}|\epsilon)$ is the probability distribution function (PDF) of these variables depending on the fit parameters $\epsilon = (\tilde{M}_D, \langle\Delta E\rangle, b_{\rm uds}, b_{DD})$:

$$\mathcal{P}(\mathbf{v}|\epsilon) = \mathcal{P}_{\rm sig}(\mathbf{v}|\tilde{M}_D, \langle\Delta E\rangle) + b_{\rm uds}\mathcal{P}_{\rm uds}(\mathbf{v}) + b_{DD}\mathcal{P}_{DD}(\mathbf{v}). \tag{4.9}$$

Here $\mathcal{P}_{\rm sig}$ is the PDF of the signal events which depends on $\tilde{M}_D$ (D mass) and $\langle\Delta E\rangle$ (the central value of the ΔE distribution), $\mathcal{P}_{\rm uds}$ is the PDF for the background process $e^+e^- \to q\bar{q}$ ($q = u, d, s$), and $\mathcal{P}_{DD}$ is the PDF for the background from $e^+e^- \to D\overline{D}$ decays with D decaying to all modes other than the signal one, $b_{\rm uds}$ and b_{DD} are their relative magnitudes. The $\mathcal{P}_{\rm sig}$, $\mathcal{P}_{\rm uds}$ and $\mathcal{P}_{DD}$ PDFs are obtained using parameterization of MC distributions.

5 Analysis of $D^0 \to K^-\pi^+$

Multihadron candidates which contain at least three tracks close to the interaction region (transverse distance from the beam R <5 mm, and longitudinal distance $|z|$ <120 mm) forming a common vertex are selected at the first stage of the analysis. The pairs of oppositely charged tracks are taken as D^0 decay candidates with the following requirements:

- Number of track hits $N_{\rm hits}$ ≥24,
- Track fit quality χ^2 <100,
- Transverse momentum: 100< p_T <2000 MeV,
- Energy of the associated cluster in the calorimeter E <1000 MeV.

For a proper calculation of $\Delta E = E_\pi + E_K - E_{\rm beam}$, π/K identification is needed. The tracks from $D^0 \to K^-\pi^+$ decay have mean momentum near 800 MeV/c. During data taking of the first data sample in 2004 only one layer of ACC was installed in the KEDR detector. It did not provide the sufficient efficiency and was not used. Fortunately, since the D meson momentum is small, the difference between K and π momenta is not large thus the error in the D-meson energy due to the incorrect mass assignment does not exceed 30 MeV. Thus, we take the following combination as a D meson energy:

$$E' = (E_{K^-\pi^+} + E_{K^+\pi^-})/2, \tag{5.1}$$

where

$$\begin{aligned} E_{K^-\pi^+} &= \sqrt{M_K^2 + p_-^2} + \sqrt{M_\pi^2 + p_+^2}, \\ E_{K^+\pi^-} &= \sqrt{M_K^2 + p_+^2} + \sqrt{M_\pi^2 + p_-^2}. \end{aligned} \tag{5.2}$$

The energy E' calculated this way is practically unbiased from the true energy E. For analysis of the second data sample π/K identification with two layers of aerogel Cherenkov counters was employed. The technique of π/K identification is described in detail in [18, 19]. For the second data sample the mean π/K separation quality is 2.8σ for a threshold of 1 ph.e. The use π/K identification allows to increase the signal-to-background ratio by approximately 2 times. The main contribution of PID is the suppression of combinatorial background. The π/K identification requirements are quite loose. If the track passes through the area of geometric inefficiency of ACC system, then we leave both hypothesis (π or K) this track for D^0 meson reconstruction.

Simulation of signal events is performed with the MC generator for $e^+e^- \to D\overline{D}$ decays where D-meson decays are simulated with the JETSET 7.4 package [20], and the radiative corrections are taken into account in both initial (ISR, using the RADCOR package [21] based on Kuraev-Fadin work [22]), and final states (FSR, the PHOTOS package [23]). ISR corrections use the $e^+e^- \to D\overline{D}$ cross section energy dependence measured by the BESIII collaboration [16, 17].

The full width of the beam energy distribution was about 1.3 MeV due to variations of the VEPP-4M operation regime. To model the corrections due to ISR to account for the position on the curve describing the dependence of the cross-section on energy, the beam energy distribution in the experimental runs was divided into 10 bins. For each bin the simulation was performed with the appropriate beam energy value and accounted with a weighting factor proportional to the integrated luminosity. In calculating M_{bc} and ΔE the luminosity-weighted average beam energy is used in the simulation, while for the data beam energy is taken for each experimental run. The beam energy in simulation is determined independently and have different values for first and second data sample. The energy spread σ_W about 1.15 MeV for the first and up to 1.59 MeV for the second data samples respectively was taken into account.

The full simulation of the KEDR detector is performed using the GEANT 3.21 package [24].

The PDF of the signal events $\mathcal{P}_{\rm sig}$ depending on three variables $M_{\rm bc}$, ΔE and $\Delta|p|$ was obtained by fitting of the 3D Monte Carlo distribution obtained for given D-meson mass $M_{\rm D}$ and beam energy. It was parameterized with

$$\begin{aligned}\mathcal{P}_{\rm sig}(M_{\rm bc},\Delta E,\Delta|p|) &= |1+k_1\Delta|p|^2| \\ &\times \left[\exp\left(\frac{-(\Delta E-\langle\Delta E\rangle)^2}{2{\sigma_1}^2_{\Delta E}}\right)\times\frac{\exp\left(\frac{-(M_{\rm bc}-\langle M_{\rm bc}\rangle-cor_1\times(\Delta E-\langle\Delta E\rangle))^2}{2{\sigma_1}^2_{M_{\rm bc}}}\right)}{(\sigma_L(M_{\rm bc})+\sigma_R(M_{\rm bc}))}\right. \\ &\left.+\,|k_2|\exp\left(\frac{-(\Delta E-\langle\Delta E\rangle)^2}{2{\sigma_2}^2_{\Delta E}}\right)\times\frac{\exp\left(\frac{-(M_{\rm bc}-\langle M_{\rm bc}\rangle-cor_2\times(\Delta E-\langle\Delta E\rangle)-M_{\rm bcshift})^2}{2{\sigma_2}^2_{M_{\rm bc}}}\right)}{\sigma_{2M_{\rm bc}}}\right] \\ &+\,|k_3|\mathcal{P}_{DD}(M_{\rm bc},\Delta E,\Delta p,DDbkg\_par),\end{aligned} \tag{5.3}$$

where

$$\begin{aligned}\sigma_L(M_{\rm bc}) &= \sqrt{{\sigma_{0l}}^2_{M_{\rm bc}}+(\Delta p\times\sigma_{3M_{\rm bc}})^2+(\Delta p^2\times\sigma_{4M_{\rm bc}})^2}, \\ \sigma_R(M_{\rm bc}) &= \sqrt{{\sigma_{0r}}^2_{M_{\rm bc}}+(\Delta p\times\sigma_{3M_{\rm bc}})^2+(\Delta p^2\times\sigma_{4M_{\rm bc}})^2}, \\ \Delta M_{\rm bc} &= M_{\rm bc}-\langle M_{\rm bc}\rangle-cor_1\times(\Delta E-\langle\Delta E\rangle), \\ \Delta M_{\rm bc}<0 &: \sigma_{1M_{\rm bc}}=\sigma_L(M_{\rm bc}), \\ \Delta M_{\rm bc}>0 &: \sigma_{1M_{\rm bc}}=\sigma_R(M_{\rm bc}),\end{aligned}$$

and k_i, $\langle\Delta E\rangle$, $\langle M_{\rm bc}\rangle$, cor_1, cor_2, $\sigma_{1\Delta E}$, $\sigma_{2\Delta E}$, $M_{\rm bcshift}$, $\sigma_{2M_{\rm bc}}$, $\sigma_{0lM_{\rm bc}}$, $\sigma_{0rM_{\rm bc}}$, $\sigma_{3M_{\rm bc}}$, $\sigma_{4M_{\rm bc}}$ were fit parameters, $DDbkg\_par$ is a list of parameters of the PDF form for $D\overline{D}$ background. It is parameterized with the sum of two two-dimensional Gaussian distributions in $M_{\rm bc}$ and ΔE (representing the core and the tails of the distribution) with a correlation and with the quadratic dependence of the $M_{\rm bc}$ resolution on $\Delta|p|$. The core distribution is asymmetric in $M_{\rm bc}$ (with the resolutions $\sigma_L(M_{\rm bc})$ and $\sigma_R(M_{\rm bc})$ for the left and right slopes, respectively). The $\Delta|p|$ distribution is uniform with a small quadratic correction and with the kinematic constraint $(\Delta|p|)^2<E^2_{\rm beam}-M^2_{\rm bc}$. The parameters of the signal distribution are obtained from the fit to the simulated signal sample (figure 3).

The background from the continuum $e^+e^-\to q\bar{q}$ process (where $q=u,d,s$) is simulated using the JETSET 7.4 $e^+e^-\to q\bar{q}$ generator. The PDF is parameterized as

$$\mathcal{P}_{\rm uds}(M_{\rm bc},\Delta E,\Delta|p|)=\exp\left(-k_1\left(\frac{M^2_{\rm bc}}{E^2_{\rm beam}}-1\right)-k_2\Delta E\right)\times(1+k_3\Delta|p|^2) \tag{5.4}$$

where k_i are fit parameters. The threshould behavior at kinematic limit at $M_{\rm bc}=E_{\rm beam}$ is provided by the vernishing phase space with the constraint $\Delta|p|^2<E^2_{\rm beam}-M^2_{\rm bc}$. The result of the fit to the simulated continuum $e^+e^-\to q\bar{q}$ background is shown in figure 4.

The effect of difference in fit functions and MC distributions (seen in figure 3 and 4) is taken into account by systematic uncertainty of signal and background PDF, where an alternative forms is used.

JHEP11(2025)001

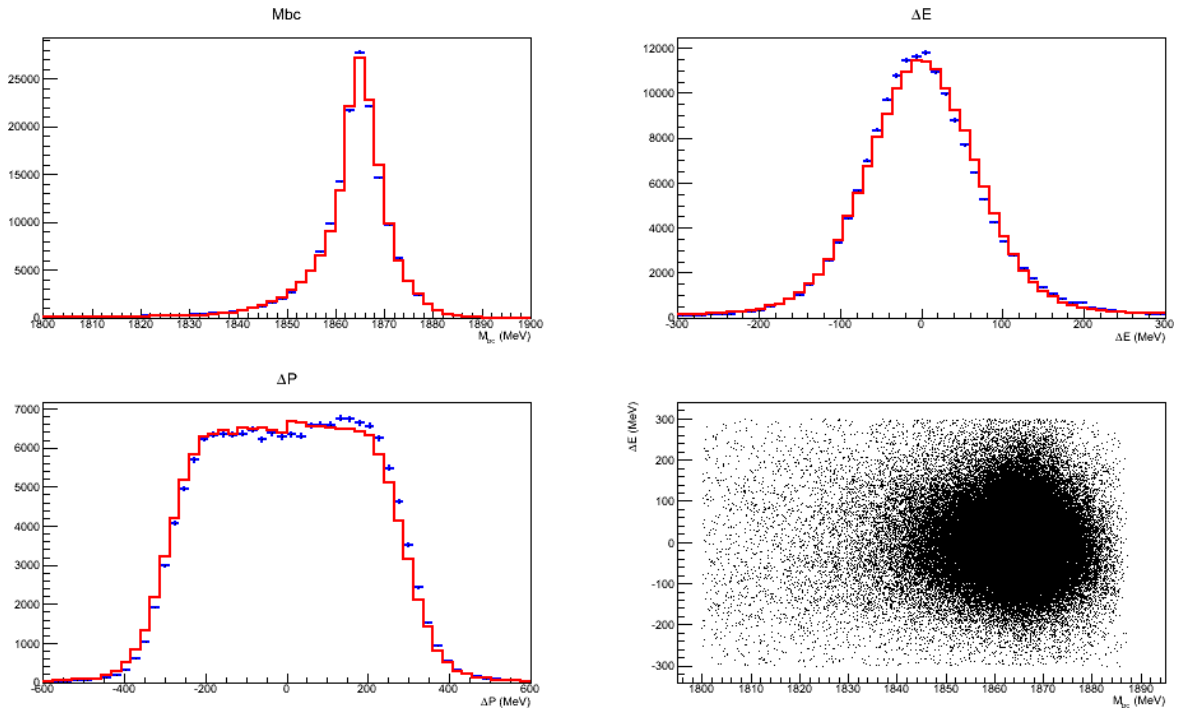

Figure 3. The distributions of $M_{\rm bc}$, ΔE, $\Delta|p|$ and correlation $M_{\rm bc}$–ΔE from MC simulated signal sample. The blue dots with error bars are from MC simulation, the solid red line is the fitting result.

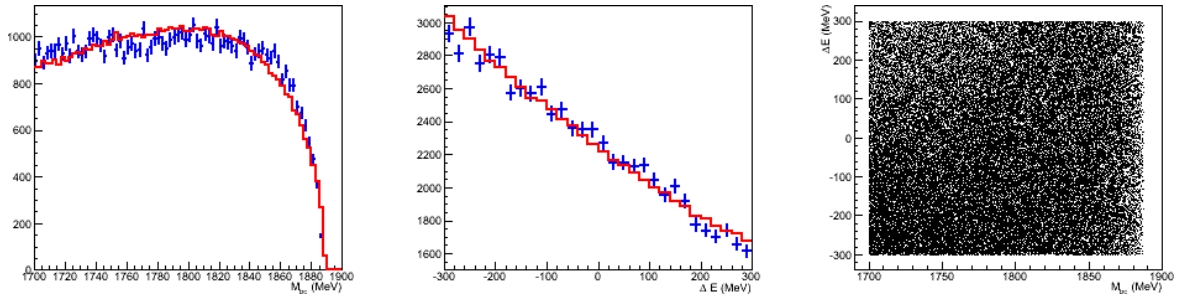

Figure 4. The distributions of $M_{\rm bc}$, ΔE and correlation $M_{\rm bc}$–ΔE from MC simulated continuum $e^+e^- \to q\bar{q}$ (where $q = u, d, s$) background sample. The blue dots with error bars are from MC simulation, the solid red line is the fitting result.

The background from $e^+e^- \to D\overline{D}$ decays is simulated using the JETSET 7.4 generator, where the signal process $D^0 \to K^-\pi^+$ is suppressed in the decay table. The PDF for $D\overline{D}$ background is parameterized with the function $\mathcal{P}_{\rm DDbkg}$ of the same form as for $\mathcal{P}_{\rm uds}$, with the addition of three two-dimensional Gaussian distributions in $M_{\rm bc}$ and ΔE. Two of them describe the background from $D^0 \to \pi^+\pi^-$ and $D^0 \to K^+K^-$, while the third one is responsible for the decays of D mesons to three and more particles. The PDF form for

JHEP11(2025)001

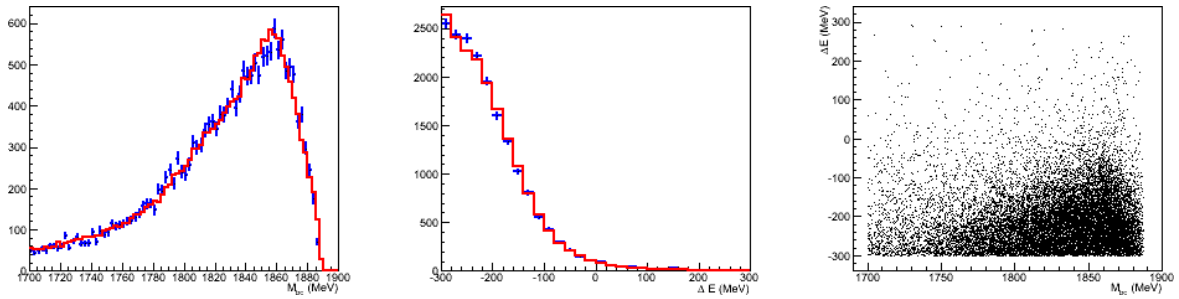

Figure 5. The distributions of $M_{\rm bc}$, ΔE and correlation $M_{\rm bc}$–ΔE from MC simulated $D\overline{D}$ background sample. The blue dots with error bars are from MC simulation, the solid red line is the fitting result.

$D\overline{D}$ background is presented below

$$\begin{aligned}\mathcal{P}_{\rm DDbkg}(M_{bc},\Delta E,\Delta|p|) = &\left(\exp\left(k_1\left(\frac{M_{bc}^2}{E_{\rm beam}^2}-1\right)-k_2\Delta E\right)\right.\\ &+|k_3|\exp\left(-\frac{(M_{bc}-\langle M_{bc0}\rangle)^2}{2\sigma_{0M_{bc}}^2}-\frac{(\Delta E-\langle\Delta E_0\rangle)^2}{2\sigma_{0\Delta E}^2)}\right)\\ &+|k_4|\exp\left(-\frac{(M_{bc}-\langle M_{bc1}\rangle-M_{\rm bcshift})^2}{2\sigma_{1M_{bc}}^2}-\frac{(\Delta E-\langle\Delta E_1\rangle)^2}{2\sigma_{1\Delta E}^2}\right)\\ &\left.+|k_5|\exp\left(-\frac{(M_{bc}-\langle M_{bc1}\rangle+M_{\rm bcshift})^2}{2\sigma_{2M_{bc}}^2}-\frac{(\Delta E+\langle\Delta E_1\rangle)^2}{2\sigma_{2\Delta E}^2}\right)\right)\times|1+k_6\Delta|p|^2|,\end{aligned}\tag{5.5}$$

where k_i, $\langle M_{bc0}\rangle$, $\langle\Delta E_0\rangle$, $\sigma_{0M_{bc}}$, $\sigma_{0\Delta E}$, $\langle M_{bc1}\rangle$, $\langle\Delta E_1\rangle$, $M_{\rm bcshift}$, $\sigma_{1M_{bc}}$, $\sigma_{1\Delta E}$, $\sigma_{2M_{bc}}$, $\sigma_{2\Delta E}$ are fit parameters. The result of the fit to the simulated $D\overline{D}$ background is shown in figure 5.

The result of the fit to the experimental data is shown in figure 6. The fitting function was written in the form (4.9) with the free parameters $\tilde{M}_D$, $\langle\Delta E\rangle$, $b_{\rm uds}$ and b_{DD} described above. The momentum correction coefficient α is chosen to keep the value of $\langle\Delta E\rangle$ close to zero. Event selection is performed with α=1.030±0.004 for the first and with α=1.013±0.003 for the second data samples respectively. To obtain the D^0 mass, one has to take into account a possible deviation of the fit parameters $\tilde{M}_D$ and $\langle\Delta E\rangle$ from the true D^0 mass and energy. In particular, the central value of $\tilde{M}_D$ can be shifted due to the asymmetric resolution function and radiative corrections. For the second dataset the shift value is 70 keV. This deviation is corrected using the MC simulation. The absolute value of the fitting parameter $\tilde{M}_D$ should be considered as a shift relative to the parameter obtained in the simulation with known initial data. For this purpose, the following correction is made:

$$M_D = M_D(PDG) + (\tilde{M}_D - \langle M_{\rm bc}\rangle),\tag{5.6}$$

where $M_D(PDG)$ is the D-meson mass from PDG included in the MC simulation, $\tilde{M}_D$ is the fit parameter from (4.9) and $\langle M_{\rm bc}\rangle$ is the fit parameter from (5.3). The results after corrections are shown in table 1. The numbers of events are presented for the region $M_{bc} > 1700$ MeV, $|\Delta E| < 300$ MeV. As can be seen from table 1, the ratio of the number of signal events of the two data samples is 1.83 and does not correspond to the ratio of the integrated luminosities. Since the first data sample (2004) does not use the ACC identification system, for a correct

JHEP11(2025)001

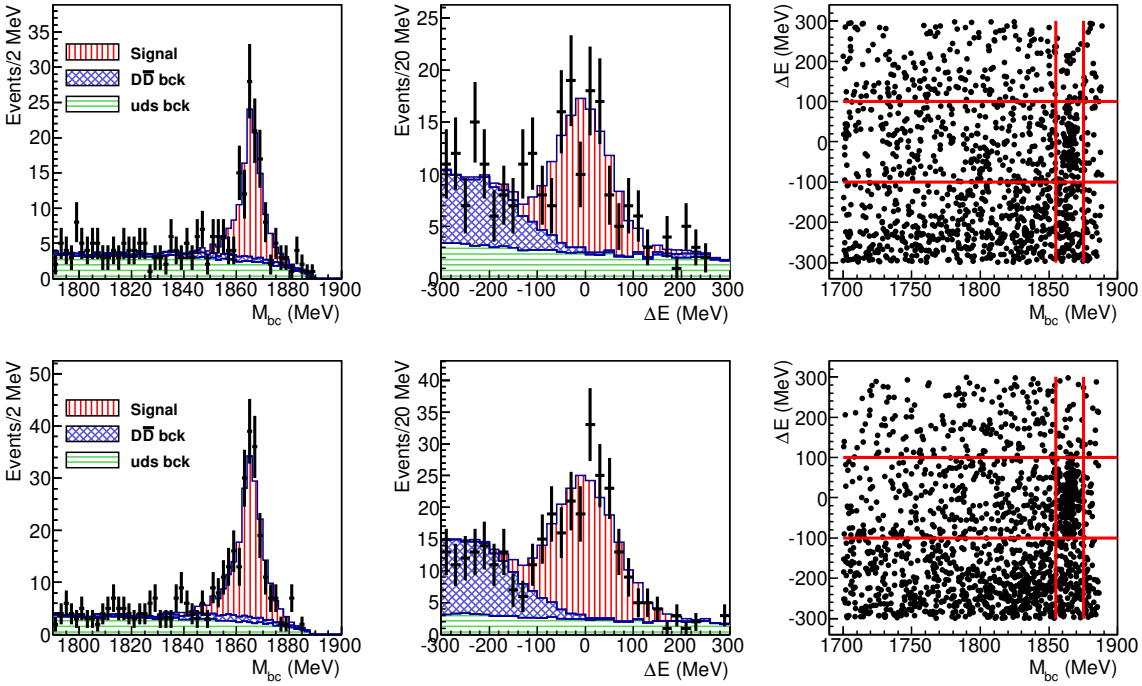

Figure 6. Experimental data (points with the error bars) and the results of the fit (histogram) for the $D^0 \to K^-\pi^+$ decay. $M_{\rm bc}$ distribution for events with $|\Delta E|$ <100 MeV (left), ΔE distribution for events with 1855 MeV< $M_{\rm bc}$ <1875 MeV (middle), and the experimental ($M_{\rm bc}$, ΔE) scatter plot (right). The top pictures correspond to the first data sample (2004), the bottom pictures correspond to the second data sample (2016–2017).

Parameter	2004	2016–2017
M_D	1865.305 ± 0.300 MeV	1864.910 ± 0.294 MeV
$\langle \Delta E \rangle$	-1.8 ± 7.5 MeV	1.0 ± 5.8 MeV
Number of signal events	118.85 ± 12.64	217.08 ± 17.18
Number of $q\bar{q}$ events	840.02 ± 89.35	841.80 ± 66.63
Number of $D\overline{D}$ events	290.13 ± 30.86	470.12 ± 37.21

Table 1. Results of the fit for the $D^0 \to K^-\pi^+$.

comparison we performed a test when the second data sample (2016–17) is processed without the ACC. For example in [19] shows comparisons of the M_{bc} distributions for the second data sample with and without the ACC system. Then the signal ratio between the two data samples becomes 2.98. The remaining inconsistency is explained by the lower track reconstruction efficiency for the second data sample (2016–17), which leads to a decrease in the D^0-meson reconstruction efficiency for the second data sample (2016–17) compared to the first data sample (2004) up to 25%. The degradation is due to the change in the state of the drift chamber and the vertex detector between the data taking periods. This effect is taken into account in the simulation.

JHEP11(2025)001

6 Analysis of $D^+ \to K^-\pi^+\pi^+$

The three-body decay $D^+ \to K^-\pi^+\pi^+$ has more kinematic parameters and there is no simple variable (such as $\Delta|p|$ in the $D^0 \to K^-\pi^+$ case), which determines the precision of the $M_{\rm bc}$ reconstruction. Therefore, we use only two variables, $M_{\rm bc}$ and ΔE, in a fit of this mode.

The mode $D^+ \to K^-\pi^+\pi^+$ does not have a problem with π/K identification for the ΔE calculation, since the sign of the kaon charge is opposite to the pion charges and thus energies of all the particles can be obtained unambiguously. The triplets of tracks with the charge of one of the tracks ("kaon") opposite to the charges of the two other tracks ("pions") are taken as $D^\pm$ decay candidates.

The requirements for the track selection are the same as in the $D^0 \to K^-\pi^+$ case. Since the significant part of the kaon tracks in the three-body decay have relatively low momentum (less than 600 MeV/c), suppression of the background from pions is possible using the TOF system and measurement of ionization losses (dE/dx) in the DC. The selection uses the following requirement on the flight time for a kaon candidate, which hits to the TOF system: $\Delta TOF = T_{\rm TOF} - T_{K(P_K)}$ >-0.8 ns (or ∼2.3 times the flight time resolution), where $T_{K(P_K)}$ is the expected flight time for a kaon with the momentum p_K and $T_{\rm TOF}$ is the measured flight time. In identification by measurement of ionization losses (dE/dx) up to five hypotheses per particle are considered (can be an electron, muon, pion, kaon or proton). The structure containing information with the probability of the particle hypothesis to be a kaon is filled. To select a kaon candidate we required that a probability hypothesis of being a kaon $P(K)$ >0.50, suppressing events located in the tail. In the second data sample analysis the Cherenkov counters were used for additional suppression of the background tracks with momentum from 450 to 1500 MeV/c. The use π/K identification allows to increase the signal-to-background ratio by approximately 1.5 times. The main contribution of PID is the suppression of combinatorial background. The π/K identification requirements are quite loose. If the track is not identified by any PID system, then we leave both hypothesis (π or K) this track for the reconstruction of the D^+-meson.

The $M_{\rm bc}$ variable uses the momenta of the daughter particles after the kinematic fit with the ΔE=0 constraint. The variable ΔE is calculated using uncorrected momenta. We select combinations that satisfy the following requirements for the further analysis: $M_{\rm bc}$ >1700 MeV, $|\Delta E|$ <300 MeV.

As in the case of $D^0 \to K^-\pi^+$ decay, simulation is performed using the $e^+e^- \to D\bar{D}$ generator taking into account ISR and FSR effects. The signal PDF $p_{\rm sig}$ is parameterized in the same way as for the $D^0 \to K^-\pi^+$ mode, but without the $\Delta|p|$ dependence.

To parameterize the continuum $e^+e^- \to q\bar{q}$ background, we use the empirical function of $M_{\rm bc}$ proposed in the Argus experiment [25] and the exponent of the quadratic form in ΔE:

$$\mathcal{P}_{\rm uds}(M_{\rm bc}, \Delta E) = y \exp\left(k_1 y^2 - [k_2 + k_3 y^2]\Delta E + k_4 \Delta E^2\right), \tag{6.1}$$

where $y = \sqrt{M_{\rm bc}/E_{\rm beam} - 1}$. The coefficients k_i were found by fitting of the MC distributions as in the D^0 case. The coefficient k_3 is responsible for the $M_{\rm bc}$ dependence of the ΔE slope, which appears after the kinematic fit to ΔE=0. The PDF for the $e^+e^- \to D\bar{D}$ background $\mathcal{P}_{\rm DDbkg}$ is parameterized with the distribution of the same form as for $\mathcal{P}_{\rm uds}$, with

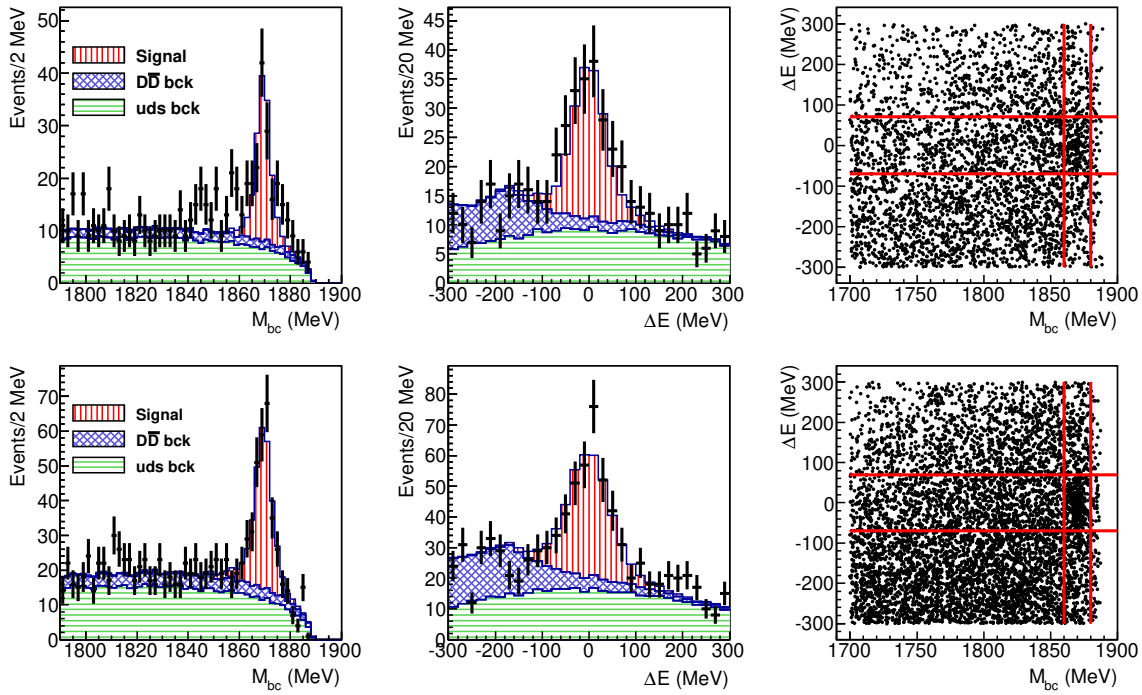

Figure 7. Experimental data (points with the error bars) and the results of the fit (histogram) for the $D^+ \to K^-\pi^+\pi^+$ decay. $M_{\rm bc}$ distribution for events with $|\Delta E|$ <70 MeV (left), ΔE distribution for events with 1860 MeV< $M_{\rm bc}$ <1880 MeV (middle), and the experimental ($M_{\rm bc}$, ΔE) scatter plot (right). The top pictures correspond to the first data sample, the bottom pictures correspond to the second data sample.

the addition of two two-dimensional Gaussian distributions in $M_{\rm bc}$ and ΔE. They describe the contributions of $D^+ \to K^+K^-\pi^+$, $D^+ \to 3\pi$ and D decays to four and more particles.

The result of the fit to the data is shown in figure 7. The momentum correction factor α is chosen such that $\langle\Delta E\rangle$ is close to zero. Event selection is performed with α=1.023±0.003 for first and with α=1.014±0.003 for second data samples respectively. The results after corrections as for D^0-meson are shown in table 2. The numbers of events are presented for the region $M_{bc} > 1700$ MeV, $|\Delta E| < 300$ MeV. Same as for the D^0-meson we can be seen from table 2 for D^+-meson that the ratio of the number of signal events of the two data samples is 1.96 and does not correspond to the ratio of the integrated luminosities. Since the first data sample (2004) does not use the ACC identification system, for a correct comparison we performed a test when the second data sample (2016–17) is processed without the ACC. For example in [19] shows comparisons of the M_{bc} distributions for the second data sample with and without the ACC system. Then the signal ratio between the two data samples becomes 3.15. The remaining inconsistency is explained by the lower track reconstruction efficiency for the second data sample (2016–17), which leads to a decrease in the D^+-meson reconstruction efficiency for the second data sample (2016–17) compared to the first data sample (2004) up to 25%. The degradation is due to the change in the state of the drift chamber and the vertex detector between the data taking periods. This effect is taken into account in the simulation.

JHEP11(2025)001

Parameter	2004	2016–2017
M_D	1869.472 ± 0.488 MeV	1869.60 ± 0.357 MeV
$\langle \Delta E \rangle$	0.4 ± 5.4 MeV	-0.3 ± 4.5 MeV
Number of signal events	178.75 ± 19.65	349.98 ± 29.04
Number of $q\bar{q}$ events	2752.27 ± 302.65	4653.36 ± 386.11
Number of $D\overline{D}$ events	633.98 ± 69.71	1624.65 ± 134.80

Table 2. Results of the fit for the $D^+ \to K^-\pi^+\pi^+$.

Source uncertainty	ΔM_{D^0}, MeV 2004	ΔM_{D^0}, MeV 2016–2017	ΔM_{D^+}, MeV 2004	ΔM_{D^+}, MeV 2016–2017
Absolute momentum calibration	0.005	0.005	0.005	0.014
Ionization loss in material	0.010	0.005	0.032	0.028
Momentum resolution	0.022	0.010	0.079	0.031
Uncertainty of meson energy	0.020	0.011	0.018	0.023
Signal PDF	0.018	0.025	0.059	0.066
Continuum background PDF	0.030	0.033	0.075	0.065
$D\bar{D}$ background PDF	0.018	0.023	0.041	0.040
PID	—	0.004	0.009	0.009
Beam energy calibration	0.007	0.005	0.005	0.003
Sum in quadrature	0.051	0.051	0.136	0.113

Table 3. Systematic uncertainties in the D^0 and D^+ mass measurements.

	2004	2016–2017
The bias of the $\langle \Delta E \rangle$ value, $D^0 \to K^-\pi^+$	1.030±0.004	1.013±0.003
The bias of the $\langle \Delta E \rangle$ value, $D^+ \to K^-\pi^+\pi^+$	1.023±0.003	1.014±0.003
$M_{K_S^0}$, $K_S^0 \to \pi^+\pi^-$	1.022±0.002	1.015±0.002

Table 4. Results of calibration of the scale coefficient α.

7 Study of systematic uncertainties

The estimates of systematic uncertainties in the D mass measurements are shown in table 3.

The contribution of absolute momentum calibration is determined by the precision of the scale coefficient α. For base result we performed calibration by measuring the average bias of the ΔE value. To estimate the systematic uncertainty, a reconstruction of the K_S^0 mass in the $\pi^+\pi^-$ channel was performed. Comparison of the mass K_S^0 found in the experiment with the PDG value one allows us to obtain a scale coefficient α to momentum. The scale coefficient obtained in various ways are presented in table 4.

As can be seen from the figure 2 the difference between the reconstructed and the true momentum due to ionization losses in the detector material can reach several MeV, so a correction to the momentum is introduced that takes it into account. The uncertainty of the simulation ionization losses in the detector material is estimated by changing the

JHEP11(2025)001

corresponding correction coefficient to the momentum. The parameters of the function (4.5) for the momentum correction were varied randomly in accordance with a Gaussian distribution with a standard deviation equal to the error of the function parameter. The effect of possible dependence of the D and κ parameters on the polar angle is taken into account in the systematic uncertainty.

The uncertainty due to the momentum resolution is estimated by using two different procedures matching the resolution in the simulation with the experimental one. The momentum resolution is adjusted using cosmic events and BhaBha events. In the first procedure the systematic error $x(t)$ of the DC given for simulation in the axial and stereo layers is multiplied by the calibration scale factors for tune the momentum resolution. In the second procedure the spatial resolution obtained by the $x(t)$ determination procedure in the axial and stereo layers is multiplied by the calibration scale factors for tune the momentum resolution.

The uncertainty in the meson energy takes into account several contributions. As noted in section 5, to model the corrections due to ISR, we take into account the energy dependence of the cross section. ISR correction uncertainty is dominated by the uncertainty of the energy dependence of the cross section $\sigma(e^+e^- \to D\bar{D})$. To estimate the systematic uncertainty value of the cross section at the measured points by energy varies randomly in accordance with a Gaussian distribution with a standard deviation equal to the statistical error of the measured cross section. In addition the difference in the energy scales of the VEPP-4M and BEPC-II [16] accelerators of about 1 MeV is acounted.

The uncertainty due to signal shape parameterization is estimated by using a single Gaussian shape instead of two ones with different widths. The continuum background shape uncertainty is estimated by using the alternative generator for the system of pions with the varying multiplicity in the simulation, and also by relaxing the background shape parameters in the experimental fit. The contribution of the $D\bar{D}$ background shape is estimated by relaxing the relative magnitude of the Gaussian shape and the non-peaking component in the experimental fit, and by excluding one of the Gaussian shapes from the background shape parameterization.

The systematic uncertainty associated with PID is determined by the probability of misidentification (pion as kaon or vice versa). Its magnitude was determined in works [18, 19, 26]. When identifying kaons or pions in the simulation, a correction was made to reproduce the misidentification probability.

The error of the beam energy calibration is dominated by the precision of the beam energy interpolation between successive energy measurements using the resonant depolarization technique. It does not exceed 60 keV. The uncertainty due to beam energy calibration is estimated as $\sigma_{E_b} = \Delta_{E_b}/\sqrt{N_{\rm sig}}$, where Δ_{E_b} — beam energy calibration error, $N_{\rm sig}$ — number of selected signal events.

Compared to the previous analysis [7] for the first data sample some systematics have been improved. First as mentioned above the systematics associated with ISR corrections has been significantly reduced by using more accurate measurements of the $\sigma(e^+e^- \to D\bar{D})$ cross section performed by the BESIII collaboration. The systematics associated with the absolute momentum calibration have been improved by using a different method for its estimation.

JHEP11(2025)001

In the current analysis we performed the calibration by measuring the average bias of the ΔE value, while to estimate the systematic uncertainty we reconstructed the K^0_S mass in the $\pi^+\pi^-$ channel. In the previous analysis contribution of absolute momentum calibration is determined by the precision of the ΔE measurement and is propagated to the uncertainty of the mass measurement using the $dM_{bc}/d\alpha$ dependence. The systematics associated with the momentum resolution have also been reduced. In the previous analysis the systematics were determined in a different way from that described above in this section. The first procedure of tuning the momentum resolution in the simulation with the experimental one corresponds to that used in the new analysis. The second procedure is different and consists of smearing the reconstructed momenta.

8 Conclusion

The masses of the neutral and charged D mesons have been measured with the KEDR detector at the VEPP-4M e^+e^- collider operated in the region of the $\psi(3770)$ meson. The analysis uses a two data samples of $0.9\,\text{pb}^{-1}$ and $4.0\,\text{pb}^{-1}$ with D mesons reconstructed in the decays $D^0 \to K^-\pi^+$ and $D^+ \to K^-\pi^+\pi^+$. To perform averaging of the results on D^0 and D^+ masses accounting for the partial correlation of systematic uncertainties we employed the procedure used in [27]. The systematic error associated with the uncertainty of the signal and background shapes is considered as the correlated part. The combination values of the masses are

$$M_{D^0} = 1865.100 \pm 0.210_{\text{stat}} \pm 0.046_{\text{syst}}\,\text{MeV},$$
$$M_{D^+} = 1869.560 \pm 0.288_{\text{stat}} \pm 0.109_{\text{syst}}\,\text{MeV}.$$

The D^0 mass value is consistent with the more precise measurements, while that of the D^+ mass is presently the most precise direct determination. These results are better than that our results published in [7] and supersedes the result in [2].

Comparison of the D meson masses obtained in this analysis with the other measurements is shown in figure 8, where KEDR 2010 — previously published result by the KEDR collaboration based on 2004 data, KEDR 2025 — weighted average result based on the collected data from 2004 and 2016–2017.

We have made a measurement of the mass difference between the D^+ and the D^0 mesons:

$$M_{D^+} - M_{D^0} = 4.46 \pm 0.36_{\text{stat}} \pm 0.12_{\text{syst}}\,\text{MeV}.$$

The systematic uncertainty is calculated under the assumption that the systematic uncertainties between the measurements of D^0 and D^+ mesons are uncorrelated. The result is in agreement with the current world average [2] and the most precise LHCb result [5].

Acknowledgments

We greatly appreciate permanent support of the staff of the experimental, accelerator and electronics laboratories while preparing and performing this experiment. The Siberian Supercomputer Center and Novosibirsk State University Supercomputer Center are gratefully acknowledged for providing supercomputer facilities.

JHEP11(2025)001

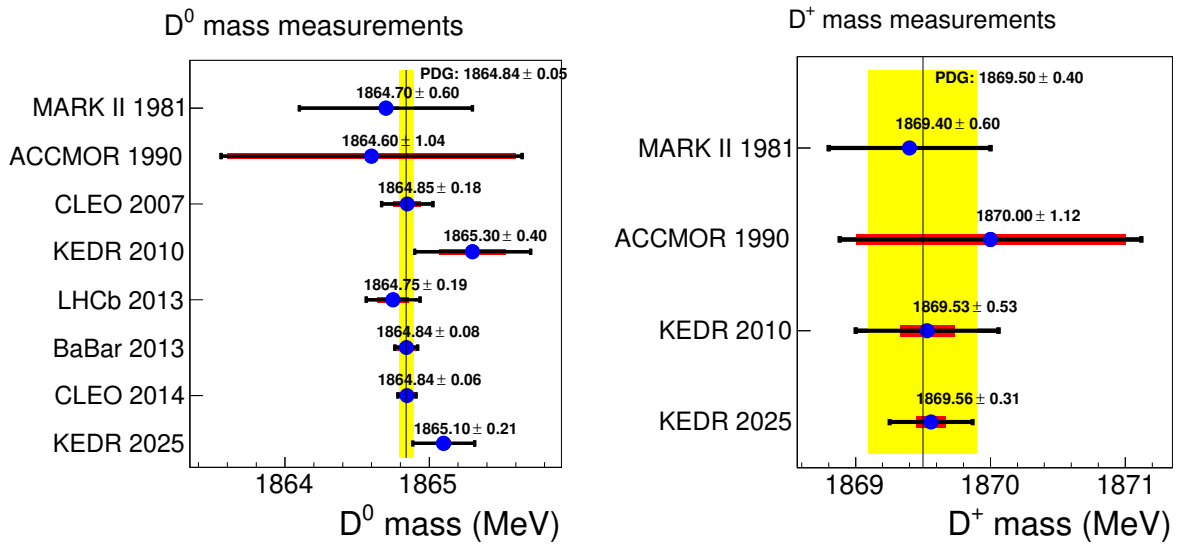

Figure 8. Comparison of published resuls on D-meson masses. The thick and thin error bars show the systematic and the total errors, respectively. The shaded areas are the PDG-2024 values [2]. The "KEDR 2025" labels correspond weighted average results based on the collected data from 2004 and 2016–2017.

Data Availability Statement. This article has no associated data or the data will not be deposited.

Code Availability Statement. This article has no associated code or the code will not be deposited.

References

[1] Y.S. Kalashnikova and A.V. Nefediev, *X(3872) in the molecular model*, *Phys. Usp.* **62** (2019) 568 [arXiv:1811.01324] [INSPIRE].

[2] Particle Data Group collaboration, *Review of particle physics*, *Phys. Rev. D* **110** (2024) 030001 [INSPIRE].

[3] A. Tomaradze et al., *High precision measurement of the masses of the D^0 and K_S mesons*, *Phys. Rev. D* **89** (2014) 031501 [arXiv:1402.1528].

[4] BaBar collaboration, *Measurement of the Mass of the D^0 Meson*, *Phys. Rev. D* **88** (2013) 071104 [arXiv:1308.1151] [INSPIRE].

[5] LHCb collaboration, *Precision measurement of D meson mass differences*, *JHEP* **06** (2013) 065 [arXiv:1304.6865] [INSPIRE].

[6] CLEO collaboration, *A Precision Determination of the D^0 Mass*, *Phys. Rev. Lett.* **98** (2007) 092002 [hep-ex/0701016].

[7] KEDR collaboration, *Measurement of D^0 and D^+ meson masses with the KEDR detector*, *Phys. Lett. B* **686** (2010) 84 [arXiv:0909.5545] [INSPIRE].

JHEP11(2025)001

[8] V.V. Anashin et al., *The KEDR detector*, *Phys. Part. Nucl.* **44** (2013) 657 [INSPIRE].

[9] V.V. Anashin et al., *Experiments with the KEDR Detector at the e^+e^- Collider VEPP-4M in the Energy Range $\sqrt{s} = 1.84$–3.88 GeV*, *Phys. Part. Nucl.* **54** (2023) 185 [INSPIRE].

[10] V.V. Anashin et al., *VEPP-4M collider: Status and plans*, in the proceedings of the *6th European Particle Accelerator Conference (EPAC 98)*, Stockholm, Sweden, 22–26 June 1998 [INSPIRE].

[11] A.D. Bukin et al., *Absolute Calibration of Beam Energy in the Storage Ring. Phi-Meson Mass Measurement*, in the proceedings of the *International Symposium on High-Energy and Elementary Particle Physics*, Warsaw, Poland, 03–09 September 1975 [INSPIRE].

[12] S.E. Baru et al., *Status of the KEDR drift chamber*, *Nucl. Instrum. Meth. A* **379** (1996) 417 [INSPIRE].

[13] V.M. Aulchenko et al., *Vertex Chamber for the Kedr Detector*, *Nucl. Instrum. Meth. A* **283** (1989) 528 [INSPIRE].

[14] A.Y. Barnyakov et al., *Operation and performance of the ASHIPH counters at the KEDR detector*, *Nucl. Instrum. Meth. A* **824** (2016) 79 [INSPIRE].

[15] A.G. Chilingarov et al., *Muon system based on streamer tubes with time difference readout*, *Nucl. Instrum. Meth. A* **265** (1988) 137 [INSPIRE].

[16] A.J. Julin, *Measurement of $D\overline{D}$ Decays from the psi(3770) Resonance*, Ph.D. Thesis, University of Minnesota (2017) [INSPIRE].

[17] BESIII collaboration, *Measurement of $e^+e^- \to D\bar{D}$ cross sections at the $\psi(3770)$ resonance*, *Chin. Phys. C* **42** (2018) 083001 [arXiv:1803.06293] [INSPIRE].

[18] A.Y. Barnyakov et al., *Particle detection efficiency of the KEDR detector ASHIPH system*, *Nucl. Instrum. Meth. A* **952** (2020) 162278 [INSPIRE].

[19] A. Yu. Barnyakov et al., *ASHIPH Cherenkov counters in the KEDR experiment*, *Nucl. Instrum. Meth. A* **1080** (2025) 170739 [INSPIRE].

[20] T. Sjostrand and M. Bengtsson, *The Lund Monte Carlo for Jet Fragmentation and e^+e^- Physics. Jetset Version 6.3: An Update*, *Comput. Phys. Commun.* **43** (1987) 367 [INSPIRE].

[21] S.E. Avvakumov et al., *UNIMOD2 — universal code for simulation of e-e+ colliding beam experiments 6. Generators of physical processes and decays of unstable particles* (in Russian), BINP preprint 2006-038 (2006).

[22] E.A. Kuraev and V.S. Fadin, *On Radiative Corrections to e^+e^- Single Photon Annihilation at High-Energy*, *Sov. J. Nucl. Phys.* **41** (1985) 466 [INSPIRE].

[23] E. Barberio and Z. Was, *PHOTOS: A Universal Monte Carlo for QED radiative corrections. Version 2.0*, *Comput. Phys. Commun.* **79** (1994) 291 [INSPIRE].

[24] R. Brun et al., *GEANT Detector Description and Simulation Tool*, CERN-W5013 (1994) [DOI:10.17181/CERN.MUHF.DMJ1] [INSPIRE].

[25] ARGUS collaboration, *Search for Hadronic $b \to u$ Decays*, *Phys. Lett. B* **241** (1990) 278 [INSPIRE].

[26] V.V. Anashin et al., *Measurement of J/ψ decays into final states $2(\pi^+\pi^-)\pi^0, K^+K^-\pi^+\pi^-\pi^0$, $2(\pi^+\pi^-)$ and $K^+K^-\pi^+\pi^-$*, *Eur. Phys. J. C* **82** (2022) 938 [INSPIRE].

[27] V.V. Anashin et al., *Measurement of main parameters of the $\psi(2S)$ resonance*, *Phys. Lett. B* **711** (2012) 280 [arXiv:1109.4215] [INSPIRE].

JHEP11(2025)001

The KEDR collaboration

V.V. Anashin[a], O.V. Anchugov[a], A.V. Andrianov[a], K.V. Astrelina[a], V.M. Aulchenko[a,b], E.M. Baldin[a,b], G.N. Baranov[a,c], A.K. Barladyan[a], A.Yu. Barnyakov[a,c], M.Yu. Barnyakov[1], S.E. Baru[a], I.Yu. Basok[a], A.M. Batrakov[a], I.V. Bedny[1], E.A. Bekhtenev[a], O.V. Belikov[a], D.E. Berkaev[a], A.E. Blinov[a,b], V.E. Blinov[a,b,c], M.F. Blinov[a], A.V. Bobrov[a,b], V.S. Bobrovnikov[a,b], A.V. Bogomyagkov[a,b], D.Yu. Bolkhovityanov[a], A.E. Bondar[a,b], D.V. Bondarev[1], A.R. Buzykaev[a,b], S.I. Eidelman[a], P.B. Cheblakov[a,b], V.L. Dorohov[a,c], F.A. Emanov[a], V.V. Gambaryan[a], Yu.M. Glukhovchenko[1], D.N. Grigoriev[a,c], V.V. Gulevich[1], D.V. Gusev[1], V.V. Kaminskiy[a,b], S.E. Karnaev[a], S.V. Karpov[a], G.V. Karpov[a], K.Yu. Karukina[a,c], D.P. Kashtankin[a], P.V. Kasyanenko[a], A.A. Katcin[a], T.A. Kharlamova[a,b], V.A. Kiselev[a], S.A. Kononov[b], K.Yu. Kotov[a], A.A. Krasnov[a], E.A. Kravchenko[a,b], V.N. Kudryavtsev[a,b], V.F. Kulikov[a,b], G.Ya. Kurkin[a], E.A. Kuper[1], I.A. Kuyanov[a,c], E.B. Levichev[a,c], P.V. Logachev[a], D.A. Maksimov[a,b], T.V. Maltsev[a], Yu.I. Maltseva[a], V.M. Malyshev[a], A.L. Maslennikov[a,b], A.S. Medvedko[1], O.I. Meshkov[a,b], S.I. Mishnev[a], I.A. Morozov[a], I.I. Morozov[a,b], N.Yu. Muchnoi[a], V.V. Neufeld[1], D.A. Nikiforov[a], S.A. Nikitin[a], I.B. Nikolaev[a,b], I.N. Okunev[a], A.P. Onuchin[1], S.B. Oreshkin[a], I.O. Orlov[1], A.A. Osipov[a,b], I.V. Ovtin[a,b,*], A.V. Pavlenko[a], S.V. Peleganchuk[a,b], K.G. Petrukhin[a], P.A. Piminov[a], S.G. Pivovarov[a,c], A.O. Poluektov[1], I.N. Popkov[1], V.G. Prisekin[a,b], O.L. Rezanova[a,b], A.A. Ruban[a,b], V.K. Sandyrev[1], G.A. Savinov[a], A.G. Shamov[a,b], D.N. Shatilov[1], L.I. Shekhtman[a], D.A. Shvedov[a], B.A. Shwartz[a,b], E.A. Simonov[a], S.V. Sinyatkin[a], Yu.I. Skovpen[a,b], A.N. Skrinsky[a], V.V. Smaluk[1], A.V. Sokolov[a,b], E.V. Starostina[a,b], D.P. Sukhanov[a], A.M. Sukharev[a,b], A.A. Talyshev[a,b], V.A. Tayursky[a,b], V.I. Telnov[a,b], Yu.A. Tikhonov[a,b], K.Yu. Todyshev[a,b], A.G. Tribendis[a,c], G.M. Tumaikin[a], Yu.V. Usov[a], A.I. Vorobiov[a], A.N. Yushkov[1], V.N. Zhilich[a,b], A.A. Zhukov[a], V.V. Zhulanov[a,b], A.N. Zhuravlev[a,b], D.A. Zubkov[a]

[a] *Budker Institute of Nuclear Physics, 11, akademika Lavrentieva prospect, Novosibirsk, 630090, Russia*
[b] *Novosibirsk State University, 2, Pirogova street, Novosibirsk, 630090, Russia*
[c] *Novosibirsk State Technical University, 20, Karl Marx prospect, Novosibirsk, 630092, Russia*

[*] *Corresponding author*
[1] *Former employee Budker Institute of Nuclear Physics.*

JHEP11(2025)001